energies

MDPI

Article

The Transient Thermal Disturbance in Surrounding Formation during Drilling Circulation

Minsoo Jang [1], Troy S. Chun [1] and Jaewoo An [2,*]

[1] Department of Petroleum Engineering, Texas A&M University, College Station, TX 77843, USA
[2] Department of Energy Science and Engineering, Stanford University, Stanford, CA 94305, USA
* Correspondence: jaewooan@stanford.edu; Tel.: +1-650-353-8071

Abstract: The injecting drilling mud is typically at the ambient temperature, relatively much colder than the deep formation, inducing a cooling effect in the formation. Although the cooled formation temperature gradually returns to its original temperature after drilling circulation, the recovery speed is slow due to low thermal diffusivity. Considering that any well tests begin in a short period after drilling ends, temperature recovery is not fully achieved before the tests. It means that the measured temperature of producing fluid is not that of the actual formation, significantly impairing the robustness of the subsequent thermal applications. Furthermore, there has been no quantified concept of thermal disturbance in the formation and its analysis. In this work, a proposed numerical transient heat transfer model computes the radial temperature in the drill pipe, annulus, and formation. The concept of quantifying thermal disturbance, named thermally disturbed radius (TDR), indicates how long the thermal disturbance occurs radially in the formation. The TDR increases with the more significant temperature difference between circulating fluid and formation. Thus, the TDR appears to be the largest at the bottom-hole depth. In the sensitivity of TDR of various operational parameters, circulation time (i.e., drilling time) is the most influential factor. Meanwhile, the other parameters do not significantly affect TDR: circulation rate, injecting mud temperature, and mud density. The sensitivity analysis concludes that as long as the operators control the drilling time, the uncertainty of the measured temperature after drilling can be manageable without limiting any other operational parameters.

Keywords: drilling circulation cooling; near-wellbore cooling; thermally disturbed radius; uncertainty of temperature

check for updates

Citation: Jang, M.; Chun, T.S.; An, J. The Transient Thermal Disturbance in Surrounding Formation during Drilling Circulation. *Energies* **2022**, *15*, 8052. https://doi.org/10.3390/en15218052

Academic Editor: Mofazzal Hossain

Received: 16 October 2022
Accepted: 27 October 2022
Published: 29 October 2022

Publisher's Note: MDPI stays neutral with regard to jurisdictional claims in published maps and institutional affiliations.

Copyright: © 2022 by the authors. Licensee MDPI, Basel, Switzerland. This article is an open access article distributed under the terms and conditions of the Creative Commons Attribution (CC BY) license (https://creativecommons.org/licenses/by/4.0/).

1. Introduction

As hydrocarbon resource consumption increases, oil and gas development is inevitable in deep-depth onshore and offshore territories. The deep-depth development poses significant challenges during the drilling process because high formation temperature causes failures in current operation designs [1]. First, all drilling facilities need to secure the operational durability of devices in a high-temperature environment, primarily electrical equipment such as logging-while-drilling and measurement-while-drilling tools, motors, and turbines [2]. Additionally, this hostile environment can also impair the performance of drilling fluids. For the appropriate operational design, there have been studies to estimate the temperature of the flowing fluids accurately in the drilling pipe and annulus [3].

The pioneering work to estimate the radial temperature distribution in the reservoir was conducted by Bullard in 1946 [4]. His work was based on a similar diffusivity equation used in a transient well test for obtaining radial pressure, and this approach became one of the major categories to compute the temperature of a reservoir analytically [5]. Edwardson et al. implemented a similar method to Bullard's but modified it to be more practical to use by applying extrapolation in the calculation process [6]. He pointed out that the circulating mud cools down the near-wellbore formation and hypothesized around 10 ft of thermal disturbance.

Later, there were works estimating the temperature distribution in consideration of more realistic conditions based on numerical methods [2,7–10]. This research illustrated a more sophisticated temperature estimation by dividing domains more and applying each domain's heat and physical properties. At first, the reservoir system was divided into two domains: wellbore and formation [7]. Later, the wellbore was subdivided into the drill pipe and annulus [8], and then it was further divided into multi-grid in the radial direction in the drill pipe [2].

In addition to considering more dividing simulation domains, there have been attempts to improve the accuracy of the temperature calculation. Gorman et al. showed sophisticated radial temperature distributions by implementing the RANS turbulent model, requiring great computing resources [11,12]. In spite of their valuable results, their work did not reveal the temperature at the payzone depth (i.e., near bottom-hole), the most important area in oil drilling. One noteworthy observation in their work is that temperature change by rotating drill pipe is minor because the axial velocity of the drilling fluid is much faster than that of the rotating drill pipe, suppressing the secondary motion induced by the rotating drill pipe [11].

In the transient well test, the temperature has been regarded as a complementary component to identifying reservoir parameters and production rate. However, with the advanced sensing platforms, several thermal applications have been developed using the measured temperature. Not only estimation techniques of production rate, but rate allocation in the multi-payzone system are introduced [13]. Furthermore, flow pattern identification through the real-time temperature data and identification of liquid condensate bank behavior was recently proposed [14].

Drilling mud is injected from the wellhead at an ambient temperature much lower than the deep formation temperature at the initial stage. Although the temperature of the circulating mud increases while it circulates through the deep reservoir, it still stays much lower compared to the deep formation temperature. Cold circulating mud takes heat from the adjacent formation, inducing a cooling effect during drilling operation [8,11]. At the formation surface facing the circulating mud (hereafter, "wellbore wall"), forced convection with a significant heat transfer rate is the dominant heat exchange component between the circulating mud and wellbore wall. On the other hand, although convection can take place in some formation parts containing a porous medium, most heat transfer inside the formation occurs only by conduction [7].

Compared to hydraulic diffusivity, thermal diffusivity is typically so low that thermal transient lasts several years even in a small reservoir with a radius of 50 m [15,16]. As conduction has the lowest heat transfer rate among the heat transfer mechanisms, it is not enough to offset the rapid temperature drop by the circulating mud [17]. Due to the imbalance of heat transfer, a thermal disturbance occurs in the radial direction inside the formation. As a result, the formation starts to cool from the near-wellbore area during the drilling operation. When the drilling operation ends, perforation is initiated after several hours of removing the remaining debris in the wellbore. During the perforation operation, the temperature sensor measures the temperature of reservoir fluids (i.e., hydrocarbon and water) coming into the wellbore. However, the measurement deviates from the actual formation temperature cooled down by circulating mud during drilling and subsequent clean-up operations.

This discrepancy in temperature can significantly degrade the accuracy of the measured temperature as well as the robustness of the thermal applications. Estimation of production rate, one of the applications using the temperature data, requires a high degree of accuracy [13]. Even a slight error in the measured temperature may make the estimated results meaningless. While the cooling effect in the formation by drilling has been mentioned in some previous research works, few papers pay attention to the risk potential of inaccurate temperature measurement [5,7,17]. Furthermore, there has been no specific concept of this thermal disturbance by drilling circulation and its analysis.

In this work, a numerical transient heat transfer model is developed to compute the radial temperature distribution in the drill pipe, annulus, and formation. Using this tool, we introduce the quantified concept of the thermal disturbance, named thermally disturbed radius (TDR), which indicates how long the thermal disturbance occurs radially in the formation (Figure 1). Lastly, through the sensitivity analysis of TDR with various conditions during drilling, we propose operational guidelines to reduce the uncertainty of temperature measurement.

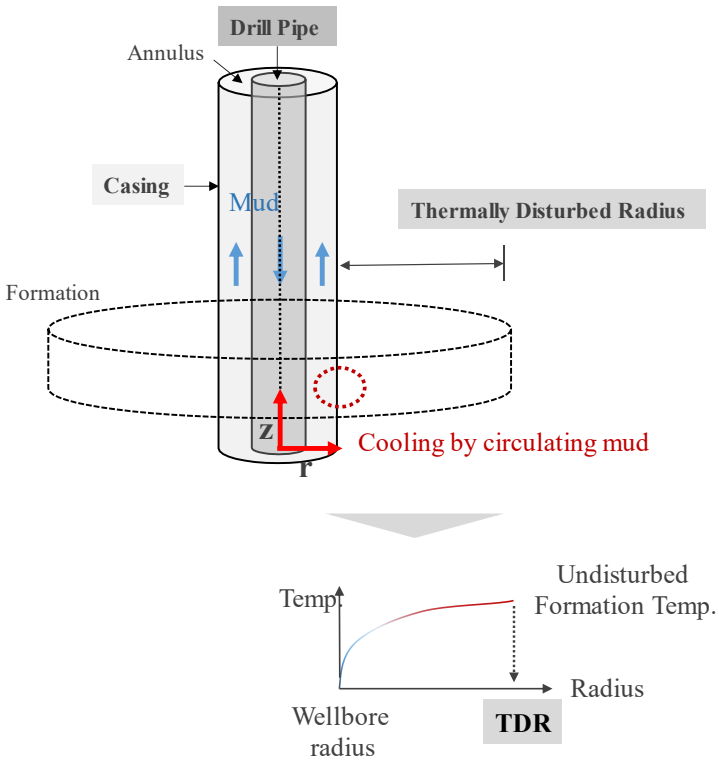


Figure 1. Schematic diagram of cooling effect by the circulating mud during drilling.

2. Methodology

2.1. Governing Equations

The operational system during drilling consists of five subsections: drilling hole (*h*), drill pipe (*p*), annulus (*a*), casing (*c*), and reservoir formation (*f*). To obtain the temperature profiles of the system, we deploy the governing equations of heat transfer balance in each section (Equation (1)). The imposed assumptions in this work are the following:

(1) Incompressible single-phase fluid (i.e., oil, no free gas);
(2) Constant heat properties;
(3) No reservoir flow;
(4) Negligible Joule–Thomson effect;
(5) The heated mud through deep formation is sufficiently cooled to the injecting temperature. The circulating mud is often observed to be heated by the circulation through the deep formation in the drilling practice; this phenomenon becomes more distinct when the circulation time gets longer.

The governing equations of heat transfer in the five sections are represented as

$$\begin{aligned} A_h h_{h,p}\frac{\partial(\rho_m c_m T_h)}{\partial t} &= L_{h,p}h_{h,p}(T_p - T_h) + A_h h_{h,p}\frac{\partial}{\partial z}\left(\lambda_m \frac{\partial T_h}{\partial z}\right) + \frac{\partial(\rho_m c_m T_h q)}{\partial z} - Q_{h,a}, \\ A_p\frac{\partial(\rho_p c_p T_p)}{\partial t} &= L_{h,p}h_{h,p}(T_h - T_p) + L_{p,a}h_{p,a}(T_a - T_p) + A_p\frac{\partial}{\partial z}\left(\lambda_p\frac{\partial T_p}{\partial z}\right), \\ A_a\frac{\partial(\rho_m c_m T_a)}{\partial t} &= L_{p,a}h_{p,a}(T_p - T_a) + L_{a,c}h_{a,c}(T_c - T_a) + A_a\frac{\partial}{\partial z}\left(\lambda_m\frac{\partial T_m}{\partial z}\right) \\ &\quad - \frac{\partial(\rho_m c_m T_h q)}{\partial z} + Q_{h,a}, \\ A_c\frac{\partial(\rho_c c_c T_c)}{\partial t} &= L_{a,c}h_{a,c}(T_a - T_c) + Q_{f,c} + A_c\frac{\partial}{\partial z}\left(\lambda_c\frac{\partial T_c}{\partial z}\right), \\ \rho_f c_f\frac{\partial T_f}{\partial t} &= \frac{1}{r}\frac{\partial}{\partial r}\left(\lambda_f r\frac{\partial T_f}{\partial r}\right) + \frac{\partial}{\partial z}\left(\lambda_f\frac{\partial T_f}{\partial z}\right). \end{aligned} \tag{1}$$

As the pipe flow is turbulent, the convection heat coefficient h is evaluated by the Dittus–Boelter equation, as shown in Equation (2).

$$\begin{aligned} h &= Nu\lambda_m/d_x \\ Nu &= 0.023Re^{0.8}Pr^{0.4}, \\ Re &= \rho_m q d_x/\mu A_x \ (x = h, a), \\ Pr &= \mu c_m/\lambda_m, \\ d_h &= 2r_h, \\ d_a &= 2(r_a - r_p), \end{aligned} \tag{2}$$

where Nu is the Nusselt number, Re is the Reynolds number, Pr is the Prandtl number, μ is the viscosity, and d is the hydraulic diameter. $Q_{f,c}$ is the heat flux from the reservoir formation to the casing:

$$Q_{f,c} = -L_{c,r}\frac{\partial}{\partial r}\left(\lambda_f r\frac{\partial T_r}{\partial r}\right)\Big|_{r=r_c} = -L_{c,r}\lambda_f\frac{\partial T_r}{\partial r}\Big|_{r=r_c}. \tag{3}$$

The radial heat transfer from the drilling hole to the annulus exists at the bottom-hole due to the mass transport. $Q_{h,a}$ is the heat flux from the drilling fluid to the annulus approximated as

$$Q_{h,a} \approx -\frac{\partial(\rho_m c_m T q)}{\partial r}\chi_{z_{bth}}, \tag{4}$$

where $\chi_{z_{bth}}$ is the step function defined with the TDR and end locations of the bottom-hole $z_{bth,\,bot}$ and $z_{bth,\,top}$ as

$$\chi_{z_{bot}} = \begin{cases} 1;\ z_{bth,bot} \le z \le z_{bth,\,top} \\ 0;\ otherwise \end{cases}. \tag{5}$$

To simplify the equations, the assumptions in the drill pipe and the casing sections are the following: the negligible vertical heat conduction and negligible heat accumulation by drilling rigs in relation to a large mass of soil. Those two assumptions lead to the same amount of heat flux inwards and outwards in those two sections. The simplified governing equation of the drill pipe is represented as

$$L_{h,p}h_{h,p}(T_h - T_p) + L_{p,a}h_{p,a}(T_a - T_p) = 0. \tag{6}$$

From this equation, we can derive the mathematical expression of T_p as a function of T_a and T_h:

$$T_p = \frac{L_{h,p}h_{h,p}T_h + L_{p,a}h_{p,a}T_a}{L_{h,p}h_{h,p} + L_{p,a}h_{p,a}}. \tag{7}$$

In the same way, the mathematical expression of T_c as a function of T_a and T_r reads

$$T_c = T_a - \frac{Q_{r,c}}{L_{a,c}h_{a,c}} = T_a - \frac{L_{c,r}\lambda_f}{L_{a,c}h_{a,c}}\frac{\partial}{\partial r}\left(r\frac{\partial T_r}{\partial r}\right)\Big|_{r=r_c} = T_a - \frac{L_{c,r}\lambda_f}{L_{a,c}h_{a,c}}\beta. \tag{8}$$

Then, by inserting Equations (7) and (8) into Equation (1), the simplified system of the governing equations is given as

$$\begin{aligned} A_h\frac{\partial(\rho_m c_m T_h)}{\partial t} &= h_{h,a}(T_a - T_h) + A_h\frac{\partial}{\partial z}\left(\lambda_m\frac{\partial T_h}{\partial z}\right) + \frac{\partial(\rho_m c_m T_h q)}{\partial z} - Q_{h,a}, \\ A_a\frac{\partial(\rho_m c_m T_a)}{\partial t} &= h_{h,a}(T_h - T_a) - L_{c,r}\lambda_f\beta + A_a\frac{\partial}{\partial z}\left(\lambda_m\frac{\partial T_m}{\partial z}\right) - \frac{\partial(\rho_m c_m T_h q)}{\partial z} + Q_{h,a}, \\ \rho_f c_f\frac{\partial T_f}{\partial t} &= \frac{1}{r}\frac{\partial}{\partial r}\left(\lambda_f r\frac{\partial T_f}{\partial r}\right) + \frac{\partial}{\partial z}\left(\lambda_f\frac{\partial T_f}{\partial z}\right), \end{aligned} \tag{9}$$

where $h_{h,a}$ is the heat transfer coefficient between the drilling hole and the annulus defined as the length-weighted harmonic average of two convection heat transfer coefficients:

$$h_{h,a} = \frac{L_{h,p}h_{h,p}L_{p,a}h_{p,a}}{L_{h,p}h_{h,p} + L_{p,a}h_{p,a}}. \tag{10}$$

The initial conditions for T_h, T_a, and T_r are assumed with the geothermal gradient g_T and the surface temperature T_{surf} as

$$T_x(r, z, t = 0) = T_{surf} - g_T z (x = h,\ a,\ f). \tag{11}$$

The boundary conditions are represented as

$$\begin{aligned} T_h(r, z = 0, t > 0) &= T_{inj}, \\ \frac{\partial T_h}{\partial z}(r, z = z_{bth,bot},\ t) &= 0, \\ T_a(r, z = 0, t) &= T_{surf}, \\ \frac{\partial T_a}{\partial z}(r, z = z_{bth,bot},\ t) &= 0, \\ T_f(r, z = 0, t) &= T_{surf}, \\ \frac{\partial T_f}{\partial z}(r, z = z_{bth,bot},\ t) &= 0, \\ T_f(r = r_e, z, t) = T_f(r = r_e, z, t = 0) &= T_e, \end{aligned} \tag{12}$$

where r_e is the reservoir boundary radius.

2.2. Numerical Scheme

In this study, we derive the numerical transient heat transfer model in a two-dimensional r-z domain to derive the TDR (Figure 2). The finite volume method is implemented for the discretization, which is known for satisfying the heat energy balance of each element. The backward difference approximation for temporal discretization is used. For spatial discretization, we calculate the first derivatives with the forward difference approximation

and the second derivatives with the central difference approximation. The governing equations in Equation (9) are discretized as

$$A_h\rho_m c_m\frac{T_{1,j}^{n+1}-T_{1,j}^{n}}{\Delta t}=h_{h,a}\left(T_{2,j}^{n+1}-T_{1,j}^{n+1}\right)+A_h\lambda_m\frac{T_{1,j+1}^{n+1}-2T_{1,j}^{n+1}+T_{1,j-1}^{n+1}}{\Delta z^2}+$$
$$\rho_m c_m q\frac{T_{1,j+1}^{n+1}-T_{1,j}^{n+1}}{\Delta z}-Q_{h,a,j}^{n+1}\ (\text{drilling hole}),$$
$$A_a\rho_m c_m\frac{T_{2,j}^{n+1}-T_{2,j}^{n}}{\Delta t}=h_{h,a}\left(T_{1,j}^{n+1}-T_{2,j}^{n+1}\right)-L_{c,r}\lambda_f\beta_j^{n+1}+A_a\lambda_m\frac{T_{2,j+1}^{n+1}-2T_{2,j}^{n+1}+T_{2,j-1}^{n+1}}{\Delta z^2}-$$
$$\rho_m c_m q\frac{T_{2,j+1}^{n+1}-T_{2,j}^{n+1}}{\Delta z}+Q_{h,a,j}^{n+1}\ (\text{annulus}),$$
$$\rho_f c_f\frac{T_{i,j}^{n+1}-T_{i,j}^{n}}{\Delta t}=\frac{\lambda_f}{(r_{i-1/2}+r_{i+1/2})/2}\frac{r_{i+1/2}T_{i+1,j}^{n+1}-(r_{i+1/2}+r_{i-1/2})T_{i,j}^{n+1}+r_{i-1/2}T_{i-1,j}^{n+1}}{\Delta r^2}+$$
$$\lambda_f\frac{T_{i,j+1}^{n+1}-2T_{i,j}^{n+1}+T_{i,j-1}^{n+1}}{\Delta z^2}\ (\text{reservoir}:\ i\ \geq 3).\tag{13}$$

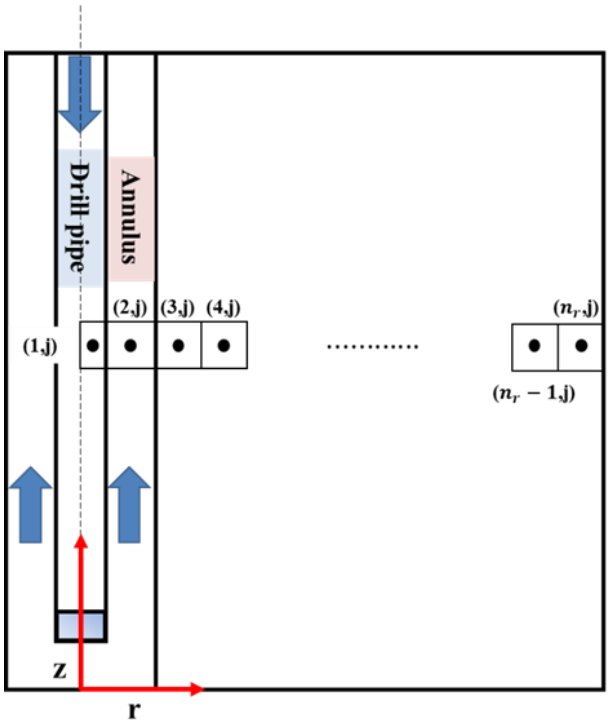


Figure 2. Scheme for numerical simulation of drill pipe, annulus, and formation.

Note that $T_h = T_{i=1}$, $T_a = T_{i=2}$, and $T_f = T_{i\geq 3}$. The subscripts i and j and the superscript n indicate indices for r, z, and t, respectively. The discretization sizes Δr, Δz, and Δt are defined as

$$\Delta r=\frac{r_e-r_c}{n_r-2},$$
$$\Delta z=\frac{|z_{bth,bot}|}{n_z},\tag{14}$$
$$\Delta t=\frac{t_{tot}}{n_t},$$

where n_t is the total number of time steps, n_r and n_z are the total number of grid cells in r and z directions, and r_i and z_j are represented as

$$r_i = \begin{cases} r_h/2, & , i = 1 \\ (r_p + r_a)/2 & , i = 2, \\ r_c + (i - 5/2)\Delta r & , i > 2 \end{cases}$$
$$r_{i+1/2} = (r_i + r_{i+1})/2, z_j = z_{bth,bot} + (j - 1/2)\Delta z, \tag{15}$$

β_j^{n+1} and $Q_{h,a,j}^{n+1}$ in Equation (13) are approximated as

$$\beta_j^{n+1} \approx \frac{1}{r_{7/2} - r_{5/2}} \left(r_{7/2} \frac{T_{4,j}^{n+1} - T_{3,j}^{n+1}}{\Delta r} - r_{5/2} \frac{T_{3,j}^{n+1} - T_{2,j}^{n+1}}{r_3 - r_2} \right),$$
$$Q_{h,a,j}^{n+1} \approx \rho_m c_m q \frac{T_{2,j}^{n+1} - T_{1,j}^{n+1}}{\Delta r} \chi_{z_{bth}}(z_j). \tag{16}$$

We developed a MATLAB-based in-house simulator to solve the numerical systems with Equations (13) and (16). With the simulator, we can derive the temperature profile at each time step. In this study, we estimate TDR from the numerical transient simulation, where

$$\frac{|T(r = TDR) - T(r = r_e)|}{T(r = r_e)} < 0.001. \tag{17}$$

Figure 3 indicates a simplified flowchart of the calculation process obtaining the temperature distribution and TDR. The temperature distribution and TDR are computed for each time step.

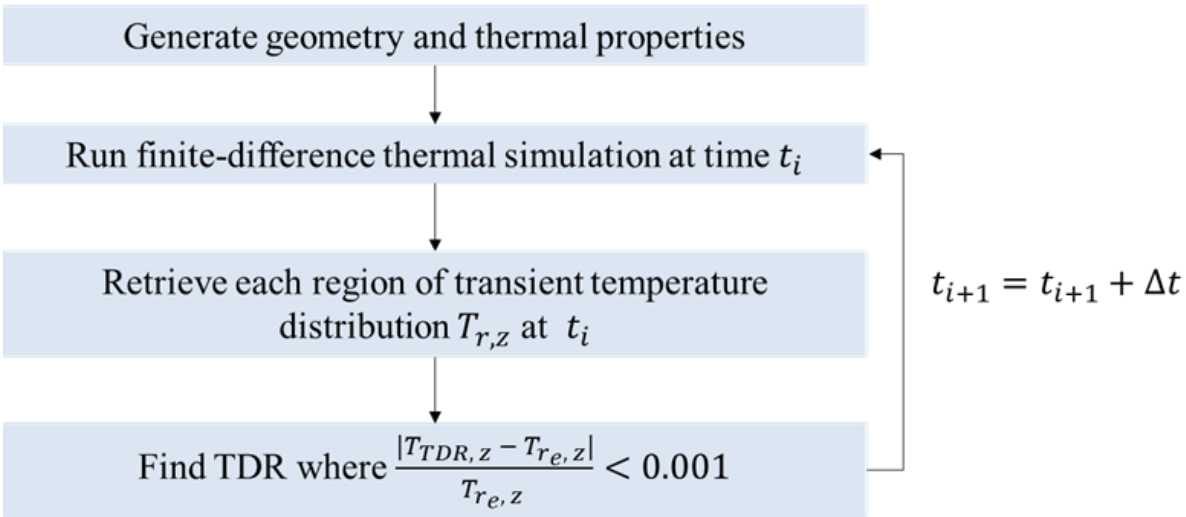


Figure 3. The flow chart of calculation.

3. Results

3.1. Validation

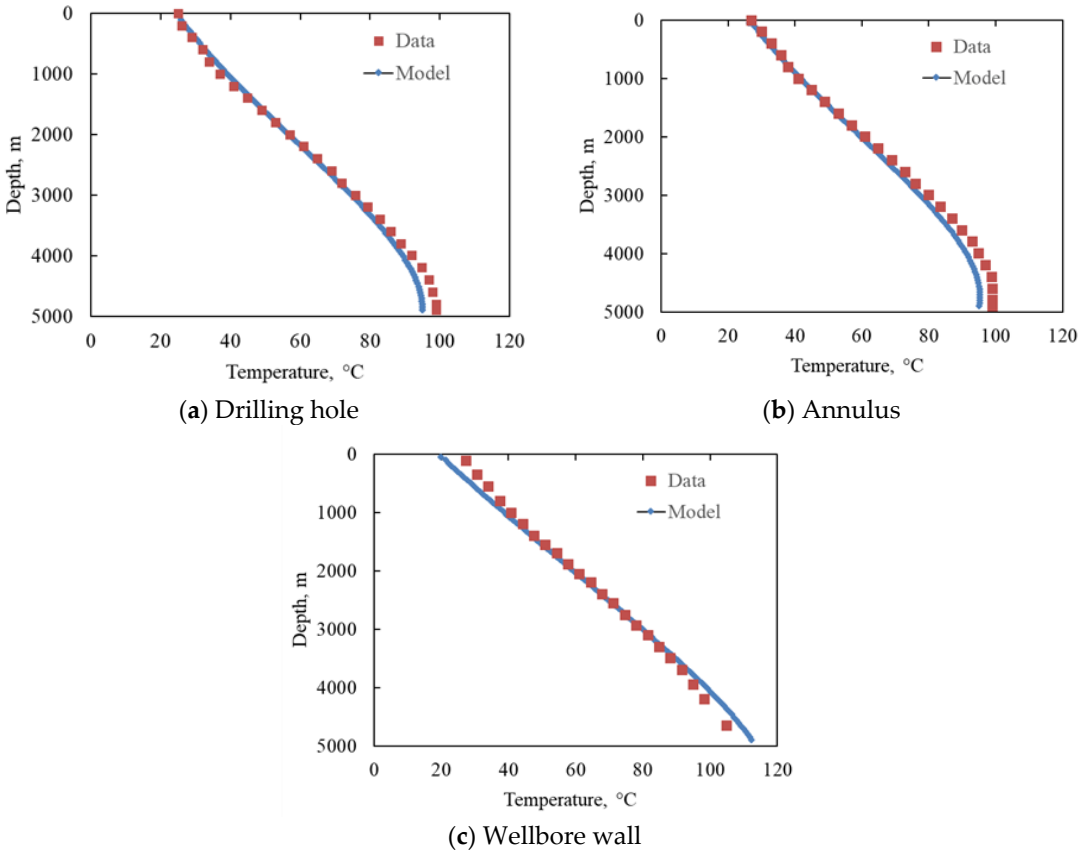
To validate the proposed transient heat transfer model, we compared the calculated temperature with the data from Yang et al.'s paper [18]. The necessary input parameters used are the same as those of Yang et al.'s work, as presented in Table 1. The model well has a total depth of 4900 m and 124 °C at the bottom-hole depth, a relatively deep high-temperature well in an operational manner. In the high-temperature well, thermal disturbance in the formation can be distinctively identified because heat exchange between the cold drilling fluid and formation remarkably occurs. The circulation time is 24 h, and the circulation rate is 18 L/s (approximately 285 gallons/min), which is the typical range

of a drilling operational condition. Considering the high formation pressure in the deep well, we use slightly heavy mud with 1.2 kg/m^3 of mud density. We assume zero casing thickness with the negligible thermal resistance of the casing.

Table 1. Parameters of drilling operation and formation.

Parameter	Value
Circulation rate, q, L/s	18
Circulation time, t_{circ}, h	24
Inlet temperature, T_{inj}, °C	25
Surface temperature, T_{surf}, °C	15
Density of the drilling mud, ρ_m, kg/m3	1200
Density of the formation, ρ_f, kg/m3	2640
Thermal conductivity of the drilling mud, λ_m, W/m. °C	1.25
Thermal conductivity of the formation, λ_f, W/m. °C	1.75
Specific heat of the drilling fluid, c_m, J/kg. °C	1600
Specific heat of the formation, c_f, J/kg. °C	800
Well depth, $\lvert z_{bth,bot} \rvert$, m	4900
Geothermal gradient, g_T, °C /100 m	2.23
Wellbore diameter, $d_a (= d_c)$, mm	210
Inner diameter of the drill pipe, d_h, mm	121.4
Outer diameter of the drill pipe, d_p, mm	139.7
Discretization levels (n_r, n_z, n_t)	(200, 100, 7)

This work describes thermal disturbance in the radial direction. We validated our radial temperature estimation at the drilling hole, the annulus, and the wellbore wall (Figure 4). Though there is a slight difference in the lower depth near the bottom hole, the overall temperature distributions in all three cases are consistent with the reference data.



(**a**) Drilling hole (**b**) Annulus

(**c**) Wellbore wall

Figure 4. Comparison of calculated temperature with reference data.

3.2. Identification of Thermal Disturbance

We identified thermal disturbance by circulating mud from the radial temperature distribution in Figure 5. The solid red and blue curves are the radial temperature at the bottom-hole depth (i.e., 4900 m) and 2000 m, respectively. The dotted gray lines are thermally undisturbed temperature (i.e., formation temperature before drilling circulation) for each depth. In Figure 5a, the temperature difference between the solid curve and the dotted line indicates how much cooling occurs in the formation by cold circulating mud. As the formation radius is much longer than the wellbore radius, the inconsistency of radial temperature varies according to the radial distance from the wellbore. The near-wellbore formation is cooled by the circulating mud. The formation temperature far from the wellbore does not change, that is, the thermal disturbance does not reach the outer boundary of the formation at this moment. The radial temperature change at the bottom hole appears to be larger than that at a depth of 2000 m.

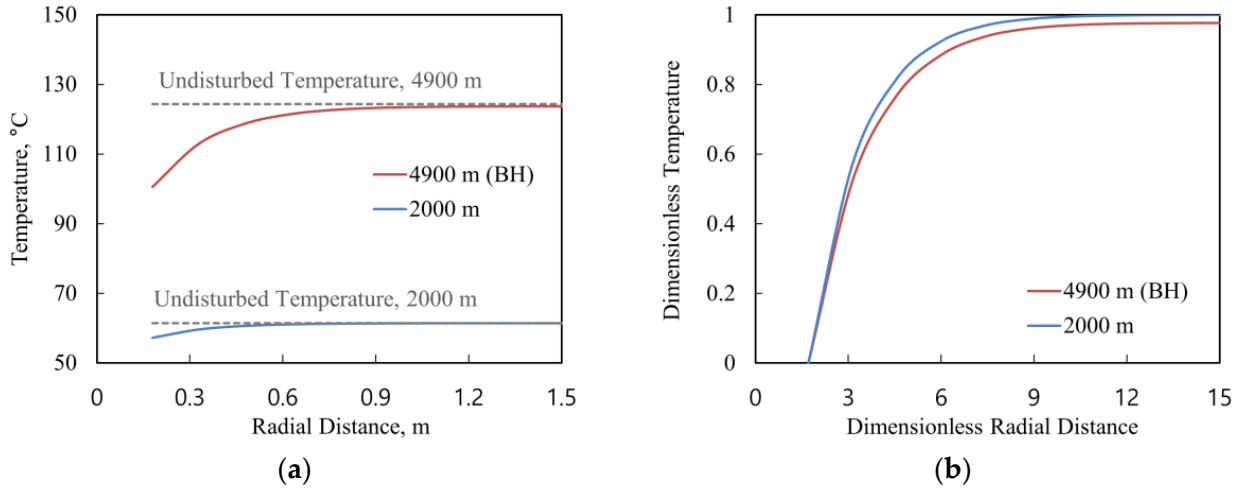


Figure 5. Radial temperature distributions of different depths: (**a**) radial temperature distribution and (**b**) dimensionless radial temperature distribution.

The radial distance and temperature were non-dimensionalized for clarity, following Equations (18) and (19), respectively. The profiles of the two curves in Figure 5b are almost identical. However, the required radial distance for converging to the undisturbed temperature (i.e., the dimensionless temperature is one) is different for each depth. When the depth is 2000 m, the curve converges to the undisturbed temperature when the radial distance is approaching 10. Meanwhile, the red curve at the bottom-hole depth does not reach even when the dimensionless radial distance is 15. The result in Figure 5b concludes that the thermal disturbance in the formation by circulating mud (i.e., TDR) is more extensive at the bottom hole than at 2000 m.

$$r_D = \frac{r}{r_c}, \tag{18}$$

$$T_D = \frac{T - T_e}{T_c - T_e}. \tag{19}$$

Figure 6 describes the thermal disturbance throughout the whole depth graphically. In this simulation, the outer reservoir boundary is 30 m, approximately 300 times the wellbore radius, which is sufficient length to describe thermal disturbance occurring over a few days. In the color map over the entire reservoir boundary (Figure 6a), the thermal disturbance is localized in the near-wellbore formation. Therefore, we represent Figure 6b as an enlarged version over $r_D \leq 30$ to visualize thermal disturbance effectively. Cooling and heating effects are determined by the temperature difference between the circulating mud and

the formation. In the upper section of the depth up to 1000 m, the formation temperature near the wellbore increases because the formation temperature in this depth range is lower than the injection temperature. As the depth rises from 1000 m, the cooling effect in the near-wellbore formation begins to appear. Thus, the thermal disturbance by the circulating inducing cooling increases with deeper depth, and its degree reaches the maximum at the bottom hole. From these observations, TDR is inferred to be increasing as the depth approaches the bottom-hole depth.

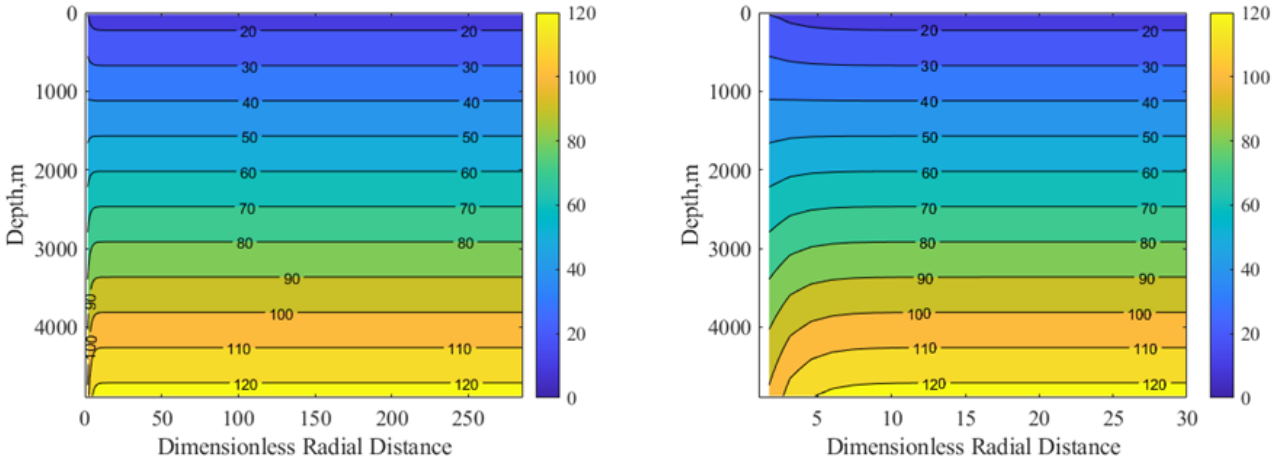


Figure 6. Temperature profiles: (**a**) a whole radial range and (**b**) an enlarged version.

4. Sensitivity Analysis

In this section, we calculate TDR along the whole depth using Equation (17) and conduct its sensitivity analysis for various operating conditions. We selected four controllable factors in operation: circulation rate, circulation time, injecting temperature, and mud density. Table 2 presents the four operational parameters for the sensitivity.

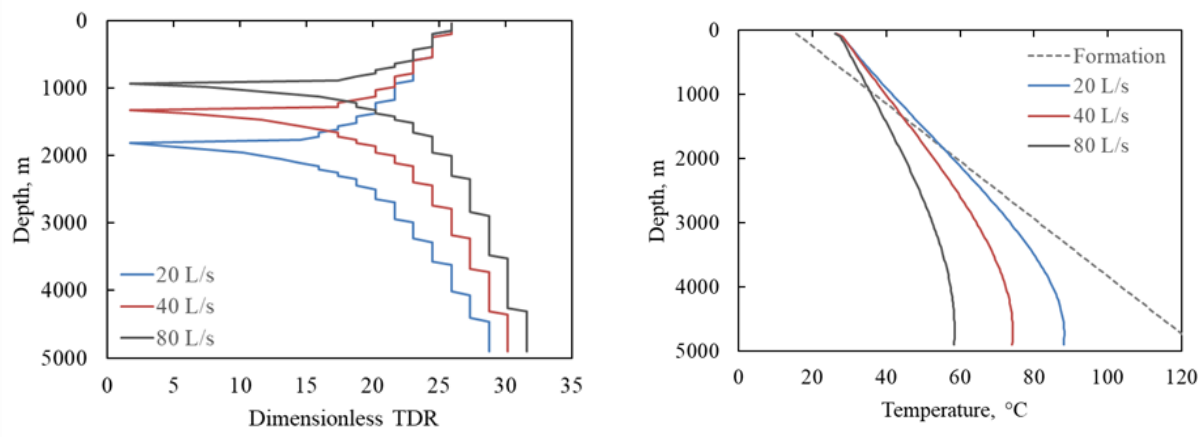
Table 2. Operational parameters for sensitivity analysis at each section.

Section	4.1	4.2	4.3	4.4
Circulation rate, q, L/s	20, 40, 80	80	80	80
Circulation time, t_{circ}, h	168	24, 72, 168	168	168
Injecting temperature, T_{inj}, °C	25	25	25, 50, 75	25
Mud density, ρ_m, 1000 kg/m3	1.2	1.2	1.2	1.0, 1.2, 1.6

4.1. Circulation Rate

Circulation rate is an indicator of the carrying capacity that can remove drilling cuttings. Therefore, it is a major factor in determining the rate of penetration (ROP) [19]. Figure 7a,b describe the TDR and fluid temperature in the annulus along with the whole well depth. The TDR is non-dimensionalized as Equation (20) for efficient comparison.

$$\mathrm{TDR_D} = \frac{\mathrm{TDR}}{r_c}. \tag{20}$$



(**a**) (**b**)

Figure 7. The sensitivity analysis of thermal disturbance with various circulation rates: (**a**) TDR and (**b**) fluid temperature in the annulus.

The circulation rate for comparison was determined to be 20 L/s, 40 L/s, and 80 L/s, shown in solid blue, red, and gray, respectively. In Figure 7a, all three TDR curves have similar shapes regardless of circulation rate. The TDR curve shape forms the minimum point at a certain depth, and below the depth, the TDR gradually increases as the depth increases. Despite the similarity of the curve shape, the minimum TDR depth of each case depends on the circulation rate. The smaller the circulation rate, the deeper the minimum TDR depth. The annulus fluid temperature can be evidence for the different minimum TDR depths, shown in Figure 7b. Because the annulus fluid is in direct contact with the formation, heat transfer occurs between the annulus fluid and the formation.

The circulation rate indicates the amount of heat capacity; the increasing fluid circulation requires more heat to change the fluid temperature. Thus, as the circulation rate increases, the temperature gradient in the annulus becomes smaller. In Figure 7b, the curve with the faster circulation deviates farther away from the formation temperature distribution (dotted gray line). Each temperature curve demonstrates a different slope intersecting the formation temperature line at different depths. The intersect depth is observed to be around 1000 m for 80 L/s, 1,400 m for 40 L/s, and 2000 m for 20 L/s, respectively. The intersect depth corresponds to the minimum TDR depth. At this depth, the heat transfer and, thus, the thermal disturbance occur minimally due to the slightest temperature difference between the circulating mud and the surrounding formation.

As observed in the previous chapter, the TDR is maximum at the bottom-hole depth in all three cases, where the temperature difference is the largest in the whole depth. The dimensionless TDR is around 28 for 20 L/s, 30.5 for 40 L/s, and 32 for 80 L/s, respectively. However, as seen from the estimated values, the increasing rate of TDR slows down compared to the rising circulation rate. Additionally, the TDR is expected to have an upper limit due to the limit of the temperature difference between the annulus fluid and the formation because the fluid temperature in the annulus cannot be lower than the injecting temperature. In conclusion, the larger circulation rate increases the TDR, but its effect is limited above a certain circulation rate.

4.2. Circulation Time

Figure 8 displays the TDR and annulus temperature distribution with various circulation times. The circulation time refers to the period of drilling and subsequent clean-up operations just before the perforation. Although circulation time can be varied significantly depending on the geologic and operational issues, one, three, and seven days of circulation are in the reasonable range in typical onshore fields. In Figure 8a, the minimum TDR depths indicate around 1000 m regardless of the different circulation times. The temperature dis-

tribution justifies this observation; the three temperature curves intersect the formation temperature line around 1000 m (Figure 8b).

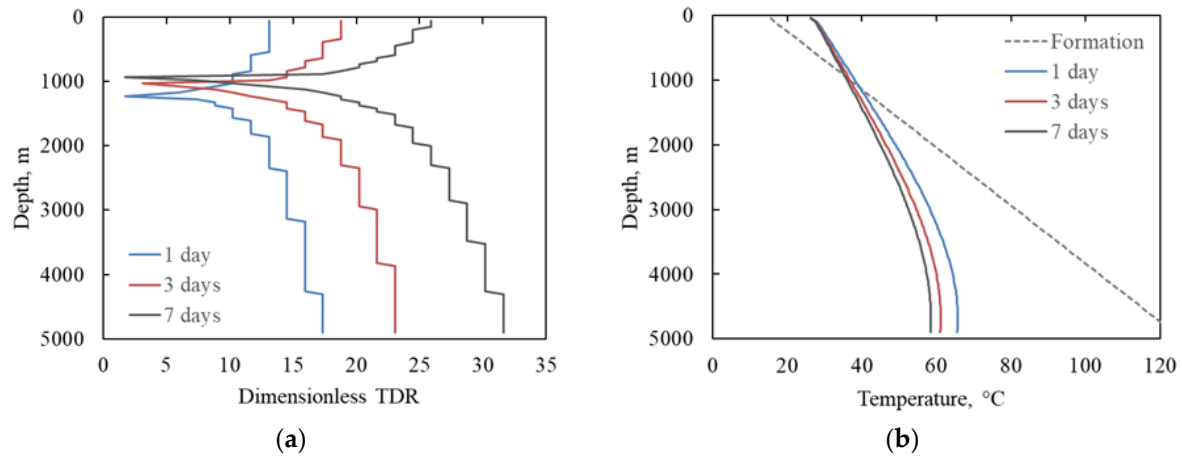


Figure 8. The sensitivity analysis of thermal disturbance with varying circulation times: (**a**) TDR and (**b**) fluid temperature in the annulus.

A noteworthy finding in Figure 8 is that the temperature variation with the various circulation times is somewhat trivial, while the TDR variation is significant. The TDR is around 17 for one day of circulation. The TDR increases almost double when the circulation lasts one week. This observation can be illustrated from the perspective of heat transfer rate in the two different domains: the formation and the wellbore wall. At the wellbore wall, the circulating mud is powered by pumps at the surface. The dominant forced convection by the pumping takes away heat from the formation. The heat removal triggers heat transfer from the outer formation boundary to the wellbore. As the fluid in the reservoir porous medium is static before the perforation, the flowability is insufficient to induce convection. Thus, conduction exists as the only heat transfer mechanism in the formation. The heat conduction in the ground is less effective than convection heat transfer in fluid. The cooling effect appears to be moving radially towards the outer boundary. The thermal disturbance continuously propagates further from the wellbore, keeping the increase in the TDR.

A lengthy circulation time leads to a large TDR, which may impair temperature measurement accuracy after drilling. The circulation time is not easily manageable because it heavily depends on the total depth and ROP. Moreover, when operational problems take place, managing the circulation time becomes even more challenging. When the circulation time becomes longer, any alternative is required to compensate for the accuracy of the measured temperature.

4.3. Injecting Temperature

Steam injection has been most widely used and effective in thermal technology [20]. The steam is injected into the wellbore to decrease the hydrocarbon viscosity. Then, it displaces the hydrocarbon towards the wellbore for production [21]. Instead of the steam injection, hot water injection can be an attractive alternative option. Though hot water injection is less efficient than the steam injection, it is more versatile even in clay-bearing reservoirs, where the steam injection cannot be implemented. The hot water injection is also more suitable for deep reservoirs with high pressure [22]. During the water injection process, controlling injecting temperature has been the primary concern in heavy oil fields.

Figure 9 shows the change in TDR and annulus temperature, the injecting temperature being at 25 °C, 50 °C, and 75 °C lower than the bottom-hole temperature (i.e., 120 °C) of this reservoir. The injecting temperature can significantly alter the minimum TDR depth, as shown in Figure 9a. When the injecting temperature increases from 25 °C to 75 °C, the minimum TDR depth changes from 1000 m to 3000 m. This result is consistent with the

depth where the temperature curves intersect the formation temperature line. Unlike the significant change in minimum TDR depth, the TDR at the bottom-hole change does not show much difference. These observations indicate that injecting temperature control can minimize the thermal disturbance at the bottom hole. If the injecting temperature is around the bottom-hole temperature with a sufficient flow rate, the minimum TDR depth can be near the bottom hole, thereby reducing temperature measurement uncertainty after drilling.

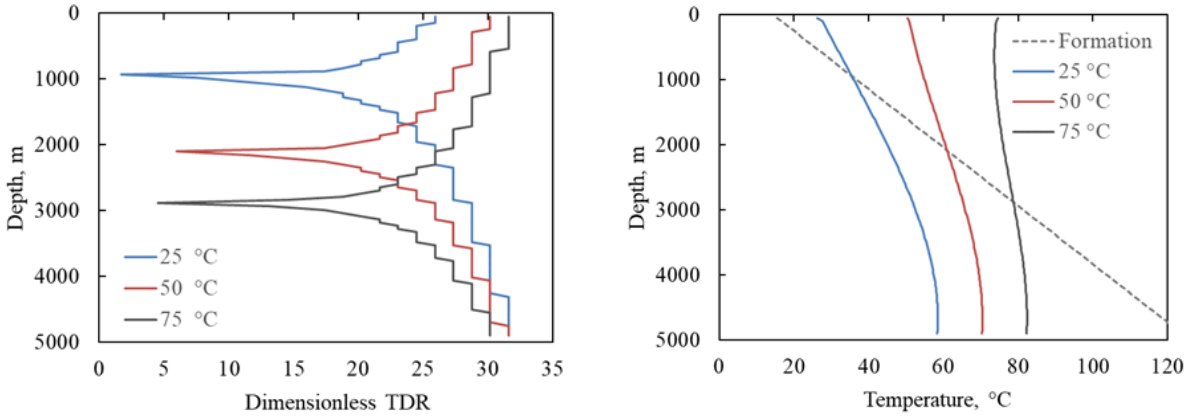


Figure 9. The sensitivity analysis of thermal disturbance with varying injection temperatures: (**a**) TDR and (**b**) fluid temperature in the annulus.

4.4. Mud Density

Mud density is one of the key operating parameters for maintaining a stable wellbore condition during the drilling operation. Using an inappropriate mud density can lead to the risk of formation fracture or/and kick [23]. Figure 10 illustrates the changes in the TDR and fluid temperature in the annulus with various mud densities. The minimum TDR depth in all three cases is around 1000 m (Figure 10a). The minimum depth is evidenced by the similar intersection points between the fluid temperature curves and the formation temperature line (Figure 10b). As the mud density becomes heavier, the TDR increases, but the increasing interval is insignificant. Mud density is the minimal influential factor among operational parameters investigated previously: circulation rate, time, and injecting temperature. Changing mud density does not impact thermal disturbance; thus, the uncertainty of temperature measurement after drilling seldom increases.

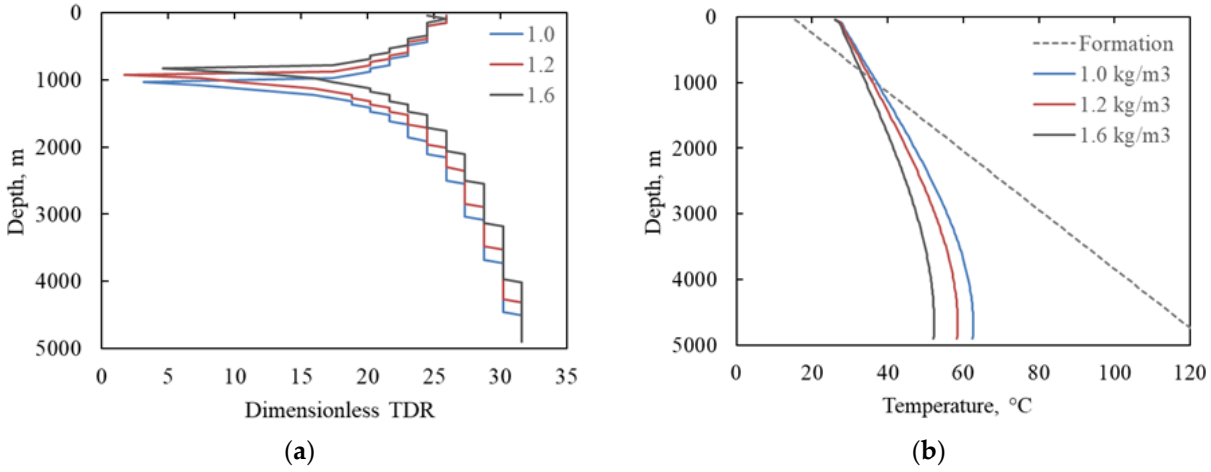


Figure 10. The sensitivity analysis of thermal disturbance with various mud densities: (**a**) TDR and (**b**) fluid temperature in the annulus.

5. Conclusions

The proposed transient heat transfer model allows us to obtain the temperature of both wellbore and formation throughout the whole well depth. A quantified concept, TDR, is introduced for quantitatively analyzing thermal disturbance in the formation. The TDR, a newly introduced concept, can be an index indicating how uncertainty can exist in the temperature measurement in any well test after a drilling operation. The following are the delivered significant insights into understanding thermal disturbance:

1. The circulating mud cools down the formation near the wellbore during drilling, causing the thermal disturbance in the formation. The TDR is the radial distance where the thermal disturbance occurs. Thus, the TDR acts as a quantified indicator of thermal disturbance.
2. The TDR tends to increase with the temperature difference between the fluids in the annulus and the formation, evidenced by the largest TDR being observed at the bottom hole.
3. Among the operational parameters, circulation time is the most influential factor in changing TDR, meaning measured temperature data may be inaccurate if the drilling operation time lasts longer. Meanwhile, other parameters (i.e., circulation rate, injecting temperature, and mud density) have insignificant effects.

Author Contributions: Conceptualization, M.J.; methodology, M.J. and J.A.; formal analysis, M.J., T.S.C., and J.A.; investigation, M.J. and J.A.; writing—original draft preparation, M.J. and J.A.; writing—review and editing, T.S.C. and J.A.; supervision, J.A. All authors have read and agreed to the published version of the manuscript.

Funding: This research received no external funding.

Institutional Review Board Statement: Not applicable.

Informed Consent Statement: Not applicable.

Data Availability Statement: The data presented in this study are available on request from the corresponding author.

Conflicts of Interest: The authors declare no conflict of interest.

Nomenclature

A	horizontal cross-sectional area, m^2
c	specific heat capacity, $J/kg - °K$
d	hydraulic diameter, m
g_T	geothermal gradient, $°K/m$
$h_{x,y}$	convection heat transfer coefficient between sections x and y, $W/m^2 - °K$
$L_{x,y}$	intersection length between sections x and y, m
	total number of grid cells in r direction
n_z	total number of grid cells in z direction
n_t	total number of time steps
Nu	Nusselt number
Pr	Prandtl number
q	well flow rate, m^3/s
$Q_{x,y}$	heat flux per unit depth from section x to section y, W/m
r	radius, m
Re	Reynolds number
t	time, s
T	temperature, $°K$
z	depth, m
λ	thermal conductivity, $W/m - °K$
Δr	radial discretization size, m
Δt	temporal discretization size, s
Δz	vertical discretization size, m

β	average temperature gradient, °K/m
μ	viscosity, pa − s
ρ	density, kg/m^3
Subscript	
a	annulus
bot	bottom
bth	bottom hole
c	casing
circ	circulation
D	dimensionless
f	formation
e	reservoir boundary
h	drilling hole
i	r-index
j	z-index
inj	injection
m	drilling mud
p	drill pipe
surf	surface
top	top
Superscript	
n	*t*-index

References

1. Wu, B.; Zhang, X.; Jeffrey, R.G. A Model for Downhole fluid and Rock Temperature Prediction during Circulation. *Geothermics* **2014**, *50*, 202–212. [CrossRef]
2. Yang, M.; Luo, D.; Chen, Y.; Li, G.; Tang, D.; Meng, Y. Establishing a Practical Method to Accurately Determine and Manage Wellbore Thermal Behavior in High-Temperature Drilling. *Appl. Energy* **2019**, *238*, 1471–1483. [CrossRef]
3. Dirksen, R. Upgrading Formation-Evaluation Electronics for High-Temperature Drilling Environments. *J. Pet. Technol.* **2011**, *63*, 24–26. [CrossRef]
4. Bullard, E.C. The Time Necessary for a Bore Hole to Attain Temperature Equilibrium. *Geophys. J. Int.* **1947**, *5*, 127–130. [CrossRef]
5. Shen, P.Y.; Beck, A.E. Stabilization of Bottom Hole Temperature with Finite Circulation Time and Fluid Flow. *Geophys. J. Int.* **1986**, *86*, 63–90. [CrossRef]
6. Edwardson, M.J.; Girner, H.M.; Parkison, H.R.; Williams, C.D.; Matthews, C.S. Calculation of Formation Temperature Disturbances Caused by Mud Circulation. *J. Pet. Technol.* **1962**, *14*, 416–426. [CrossRef]
7. Luheshi, M.N. Estimation of Formation Temperature from Borehole Measurements. *Geophys. J. R. Astron. Soc.* **1983**, *74*, 747–776. [CrossRef]
8. Espinosa-Paredes, G.; Espinosa-Martínez, E.G. A Feedback-Based Inverse Heat Transfer Method to Estimate Unperturbed Temperatures in Wellbores. *Energy Convers. Manag.* **2009**, *50*, 140–148. [CrossRef]
9. Abdelhafiz, M.M.; Hegele, L.A.; Oppelt, J.F. Numerical Transient and Steady State Analytical Modeling of the Wellbore Temperature during Drilling Fluid Circulation. *J. Pet. Sci. Eng.* **2020**, *186*, 106775. [CrossRef]
10. Kutasov, I.M.; Eppelbaum, L.V. Wellbore and Formation Temperatures During Drilling, Cementing of Casing and Shut-In. In Proceedings of the World Geothermal Congress, Melbourne, Australia, 19–25 April 2015; International Geothermal Association: Den Haag, The Netherlands, 2015.
11. Gorman, J.M.; Abraham, J.P.; Sparrow, E.M. A novel, Comprehensive Numerical Simulation for Predicting Temperatures within Boreholes and the Adjoining Rock Bed. *Geothermics* **2014**, *50*, 213–219. [CrossRef]
12. Yang, H.; Li, J.; Liu, G.; Wang, J.; Luo, K.; Wang, B. Development of Transient Heat Transfer Model for Controlled Gradient Drilling. *Appl. Therm. Eng.* **2019**, *148*, 331–339. [CrossRef]
13. Ouyang, L.B.; Belanger, D. Flow Profiling by Distributed Temperature Sensor (DTS) System—Expectation and Reality. *SPE Prod. Oper.* **2006**, *21*, 269–281. [CrossRef]
14. Jang, M. Wellbore and Near-Wellbore Heat Transfer: General Theory and Practical Application. Ph.D. Thesis, Texas A&M University, College Station, TX, USA, 2021.
15. Palabiyik, Y.; Onur, M.; Tureyen, O.I.; Cinar, M. Transient Temperature Behavior and Analysis of Single-Phase Liquid-Water Geothermal Reservoirs during Drawdown and Buildup Tests: Part I. Theory, New Analytical and Approximate Solutions. *J. Pet. Sci. Eng.* **2016**, *146*, 637–656. [CrossRef]
16. Jang, M.; Chun, T.S.; An, J. An Analytical Heat Transfer Model in Oil Reservoir during Long-Term Production. *Energies* **2022**, *15*, 2544. [CrossRef]
17. Eppelbaum, L.V.; Kutasov, I.M. Pressure and Temperature Drawdown Well Testing: Similarities and Differences. *J. Geophys. Eng.* **2006**, *3*, 12–20. [CrossRef]

18. Yang, M.; Tang, D.; Chen, Y.; Li, G.; Zhang, X.; Meng, Y. Determining Initial Formation Temperature Considering Radial Temperature Gradient and Axial Thermal Conduction of the Wellbore Fluid. *Appl. Therm. Eng.* **2019**, *147*, 876–885. [CrossRef]
19. Bridges, S.; Robinson, L. *A Practical Handbook for Drilling Fluids Processing*, 1st ed.; Gulf Professional Publishing: Houston, TX, USA, 2020.
20. Pwaga, S.; Iluore, C.; Hundseth, Ø.; Perales, F.J.; Idrees, M.U. *Comparative Study of Different EOR Methods*; Technical report; Norwegian University of Science & Technology: Trondheim, Norway, 2010.
21. Alajmi, A.F. Heat Loss Effect on Oil Bank Formation during Steam Flood. *J. Pet. Sci. Eng.* **2021**, *199*, 108262. [CrossRef]
22. Askarova, A.; Turakhanov, A.; Markovic, S.; Popov, E.; Maksakov, K.; Usachev, G.; Karpov, V.; Cheremisin, A. Thermal Enhanced Oil Recovery in Deep Heavy Oil Carbonates: Experimental and Numerical Study on a Hot Water Injection Performance. *J. Pet. Sci. Eng.* **2020**, *194*, 107456. [CrossRef]
23. Schubert, J.J.; Juvkam-Wold, H.C.; Choe, J. Well Control Procedures for Dual Gradient Drilling as Compared to Conventional Riser Drilling. *SPE Drill. Complet.* **2006**, *21*, 287–295. [CrossRef]